Appl. Phys. A (2015) 121:187–191
DOI 10.1007/s00339-015-9407-6

Applied Physics A
Materials Science & Processing

Compensation of spherical aberration influences for two-photon polymerization patterning of large 3D scaffolds

T. Stichel[1,2] · B. Hecht[2] · R. Houbertz[1,4] · G. Sextl[1,3]

Received: 30 March 2015 / Accepted: 3 August 2015 / Published online: 22 August 2015

Abstract Two-photon polymerization using femtosecond laser pulses at a wavelength of 515 nm is used for three-dimensional patterning of photosensitive, biocompatible inorganic–organic hybrid polymers (ORMOCER®s). In order to fabricate millimeter-sized biomedical scaffold structures with interconnected pores, medium numerical aperture air objectives with long working distances are applied which allow voxel lengths of several micrometers and thus the solidification of large scaffolds in an adequate time. It is demonstrated that during processing the refraction of the focused laser beam at the air/material interface leads to strong spherical aberration which decreases the peak intensity of the focal point spread function along with shifting and severely extending the focal region in the direction of the beam propagation. These effects clearly decrease the structure integrity, homogeneity and the structure details and therefore are minimized by applying a positioning and laser power adaptation throughout the fabrication process. The results will be discussed with respect to the resulting structural homogeneity and its application as biomedical scaffold.

✉ T. Stichel
tstichel@gmx.de

R. Houbertz
ruth.houbertz@multiphoton.de

[1] Fraunhofer ISC, Neunerplatz 2, 97082 Würzburg, Germany

[2] Nano-Optics and Biophotonics Group, Röntgen Research Center for Complex Material Systems, Physikalisches Institut, Lehrstuhl für Experimentelle Physik V, Julius-Maximilians- Universität, Am Hubland, 97074 Würzburg, Germany

[3] Lehrstuhl für Chemische Technologie der Materialsynthese, Röntgenring 11, 97070 Würzburg, Germany

[4] Present Address: Multiphoton Optics GmbH, Friedrich-Bergius-Ring 15, 97076 Würzburg, Germany

1 Introduction

Two-photon polymerization (2PP) in liquid resins for the realization of complex three-dimensional structures in the sub-µm range has gathered high interest in the last decade [1]. Possible applications of 2PP include the fabrication of photonic crystals [2, 3], optical waveguides [4] and optical data storage [5]. Another promising field of applications which recently has attracted considerable attention is the field of bio-medicine, where, e.g., fabrication of scaffolds and microneedles for drug delivery were demonstrated [6, 7].

2PP is based on two-photon-mediated organic cross-linking of a liquid resin with intensities that surpass a certain threshold. The use of a focused laser beam usually leads to solidification of volume pixels (voxels) in the liquid resin, whose elliptical shape relates to an iso-intensity surface of the 3D optical point spread function. Taking advantage of the threshold behavior and the nonlinearity inherent for 2PP, it is possible to even achieve sub-wavelength voxel dimensions [8, 9]. While small voxels allow to precisely fabricate fine details of a structure, the overall dimensions of such structures are usually limited to the micrometer scale because of the small working distances of commonly used immersion oil high NA objectives and the typically low polymerization rates that can be obtained. The polymerization rate is determined by the NA of the objective, the writing speed determining the exposure dose and the reactivity of the resin material. The writing speed is limited by either the reactivity of the resin material or by the technical performance of the positioning system.

In order to create objects with millimeter dimensions as required for applications as biomedical scaffolds, a drastic increase in the polymerization rate as well as an extension of the working distance has to be achieved. Recently, exposure strategies were presented which overcome the working distance limitation by providing a direct contact between the objective and the resin material [10, 11]. However, these techniques require a galvanometric mirror before the objective in order to provide high writing speeds (>10 mm/s) since the rapid relative positioning between the objective and the resin would lead to turbulences inside the resin volume.

In this paper, we demonstrate a simple approach to fabricate millimeter-sized scaffolds structures by using medium NA objectives with large working distances as well as inorganic–organic hybrid polymers (such as ORMOCER®s[1]) formulated with suitable photoinitiators that provide very high photopolymerization rates. In contrast to usually applied high NA objectives, medium NA objectives allow much larger voxel sizes due to the wider optical point spread function, leading to solidification of a larger volume in shorter time at the cost of spatial resolution. The loss in spatial resolution is especially pronounced in the axial direction due to the fact that the voxels' aspect ratios increase significantly along this axis with decreasing NA. This makes low NA objectives less useful for the fabrication of porous scaffold structures.

Hence, medium NA objectives were used in combination with highly light-sensitive and reactive cross-linkable hybrid polymer materials which allow short exposure times and thus fast scanning speeds and structures with lateral dimensions of some cm and structure heights of several mm were readily produced. Hybrid polymer/initiator systems can be designed to provide very high photoreactivity [11, 12], high mechanical stability [13], as well as a good biocompatibility [6, 14]. In order to realize large high-quality biomedical scaffolds using 2PP using a medium NA objective, we compensate defocusing and intensity loss which appear as a result of spherical aberration due to refraction of the focused beam at the air/material interface. The compensation by laser power adaptation will be discussed with respect to the resulting structural homogeneity.

2 Main experimental methods

An ytterbium laser system from Amplitude Systems (325 fs, time-averaged output power 2.5 W) which is frequency-doubled to 515 nm is used as a light source. In contrast to usual exposure techniques based on high NA immersion oil objectives, the fabrication of large-scale structures is carried out using a much lower NA (without immersion) which is displayed in Fig. 1. The liquid hybrid polymer resin is embedded in a sandwich setup consisting of two glass slides (each 170 µm thick) and a spacer which is fixed on an air-bearing stage system from Aerotech GmbH allowing movements of the sample in the x–y-plane with 1 µm accuracy and a maximum scan speed of 300 mm/s. A third stage moves the objective in the vertical direction (z). The growth process starts at the bottom glass slide (growth substrate) and proceeds toward the top glass slide.

An acrylate-based hybrid polymer labeled as ORMOCER®-V (OC-V) is used as resin for 2PP experiments. OC-V is synthesized via hydrolysis/polycondensation reactions of alkoxysilane precursors. The photoinitiator Irgacure® Oxe02 from BASF SE (2 wt%) initiates the radical chain polymerization of the organically cross-linkable groups [15]. By moving the focus through the resin, arbitrarily shaped 3D structures can be produced on surfaces or in the bulk of materials [16]. After the exposure process, the non-irradiated liquid resin can be removed by dipping the sample into a mixture of methyl isobutyl ketone and isopropanol (development), leaving the polymerized structure behind.

The maximum height of the structure is limited by the working distance of the employed objective. For the experiments, two objectives from Nikon (type: CFI S Plan Fluor ELWD) with a working distance of 8.2 mm (NA 0.45) and 3.8 mm (NA 0.60) were used, respectively. The maximum lateral extension of a fabricated scaffold structure is limited by the range of the x–y-stage to 150 × 100 mm^2. The layers consist of polymerized line gratings of a certain pitch in x/y (hatch distance) and in z (slice distance) direction. The slice and hatch distances are chosen to produce interconnected structures for a given peak intensity in the focal volume.

3 Defocussing correction

Due to the absence of an immersion oil, a high refractive index step exists at the air/glass interface, resulting in a strong defocusing effect which can be approximated by a

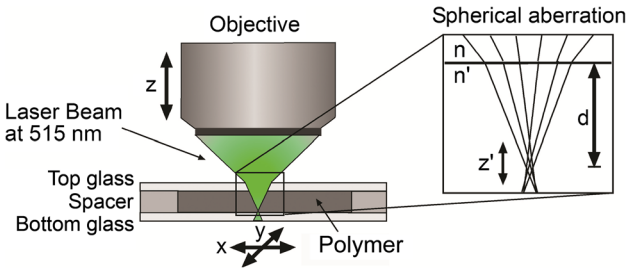

Fig. 1 Exposure strategy and spherical aberration due to refractive index mismatch

[1] ORMOCER® registered by the Fraunhofer Gesellschaft für Angewandte Forschung e. V.

formula derived straightforwardly using Snell's law of refraction for the marginal rays and subsequently replacing NA with NA/2. The latter step was done with respect to the neglected inner rays, which was confirmed by calculations using the software program PSF Lab [17]. The refraction at the glass/material interface can be ignored due approximate index matching ($n_{glas} \approx n_{resin}$). The resulting relation between axial movements of the objective z, and the actual focus position z' is given by

$$D = \frac{z'}{z} = \frac{n' \times \sqrt{1 - (\mathrm{NA}/2)^2/\mathrm{n}'^2}}{n \times \sqrt{1 - (\mathrm{NA}/2)^2/n^2}}, \quad (1)$$

where $n = 1$ is the refractive index of the surrounding area (air) and $n' = 1.52$ of the material/glass. This defocusing effect leads to an apparent stretch of software-generated large-scale 3D models during fabrication by the ratio D. With the experimental conditions which are used for the experiments, the ratio D of the intended and resulting structure height is about 1.54 for an objective with an NA of 0.45, and approximately 1.56 for an objective having an NA of 0.60. In order to compensate for this effect, a respective defocusing correction was implemented into the fabrication software. The difference between structures where the correction was employed compared to the ones without correction is obvious from Fig. 2, which shows human stapes fabricated by 2PP using an objective with an NA of 0.45 and its CAD model. The non-corrected stapes is stretched by a factor of around 1.55 which is in good agreement to the calculation of the theoretical stretching given by Eq. (1). The proportions of the corrected stapes correspond quite well to the CAD design model.

Another spherical aberration effect induced by the refractive index step is blurring of the focal photon distribution in particular along the axial (z) direction. This blurring of the point spread function leads to a reduced depth of field as well as to a lower peak intensity. Both, defocussing and blurring, increase with increasing penetration depth of the laser light into the material [17].

4 Intensity correction

The spherical aberration clearly affects the quality and homogeneity of highly porous scaffolds which can be seen in Fig. 3a. The scaffold's CAD data in Fig. 3c were designed to have a size ($l \times w \times h$) of $500 \times 500 \times 550$ µm^3 with interconnected pores of 100 µm in diameter, and it was realized at various exposure powers P with an objective having an NA of 0.60. The fabrication time for each scaffold was 18 min using a writing speed of 2.5 mm/s, and a hatch and slice distance of 5 µm.

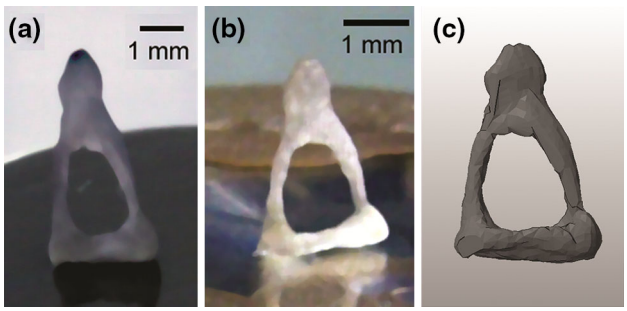

Fig. 2 **a**, **b** Human stapes produced in OC-V (formulated with 2 wt% photoinitiator) by 2PP using a NA of 0.45 **a** without and **b** with defocusing correction and **c** CAD model of human stapes

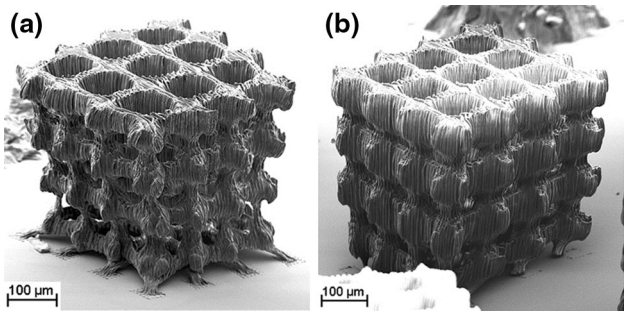

Fig. 3 SEM images of scaffolds, produced in OC-V (formulated with 2 wt% photoinitiator) with an average laper power P of **a** 2 mW, and **b** 2.5 mW

When examining the scaffold of Fig. 3a, a structural inhomogeneity along the z axis can be observed. The overall scaffold shape brings to mind an upside-down trapezoid, except for the small zone of the bottom rows of the scaffolds' pillars which are strongly bent toward the center of the scaffold regarding to the scaffolds attachment points on the bottom glass substrate. These points resemble the original structure geometry which was realized by the 2PP process.

Generally, shrinkage takes place upon cross-linking processes [2]. During the 2PP, each voxel shrinks to the same extent and remains exactly at the position of the laser focus, thus not affecting the structure's geometry. However, after the removal of the unexposed material, the drying process leads to distortion/collapse of the structure's geometry which results in the shape described above.

The distorted shape can be explained by two different effects which superimpose each other.

At the bottom glass substrate, distortion of the adherent scaffold is hindered which leads to strongly bent pillars for the bottom row. Above that, distortion is affected by the inhomogeneous degree of cross-linking along the z axis. Because the degree of cross-linking is higher in upper parts of the structure due to a distorted focus, the collapse/distortion there is much less than in the lower parts.

The inhomogeneous degree of organic cross-linking can be related to an inhomogeneous deposition of laser power along the z axis, which is caused by the influence of spherical aberration in the sense, the larger the penetration depth d into the material, the stronger the aberration and the lower the maximum peak intensity. Consequently, a lower laser power at the scaffold parts close to the bottom glass substrate leads to a lower degree of organic cross-linking.

In order to investigate and quantify the influence of spherical aberration and to improve the structure quality and homogeneity, the threshold laser power at different penetration depth was determined. To this end, single lines at different penetration depth d and different laser powers P, which represents the maximum peak intensity of the PSF, were fabricated with the NA 0.60 objective and a constant writing speed of 0.5 mm/s. By means of a live monitoring system (consisting of a red light, a dichroic mirror and a PC ocular), the threshold powers P_{th} (the power at which the first line could be recognized) were determined in situ for different penetration depth d. The results are displayed in Fig. 4a. With a linear approximation for the threshold power ($P_{\text{th}}(d) = m * d + P_0$), the slope m is 0.23 mW/mm and $P_0 = P_{\text{th}}(d = 0)$ (air/glass interface), is 155 µW. This can be correlated to a loss of laser power $1 - P_0/P_{\text{th}}(d)$ with increasing d which is plotted in Fig. 4b.

Using the data of Fig. 4a, a linear relation between $P_{\text{th}}(d)$ and the applied laser power $P(d)$ can be derived. We obtain

$$P(d) = \frac{P*}{P_0} \cdot P_{\text{th}}(d), \tag{2}$$

with $P*$ the actual laser power deposited in the focal area. Hence, the laser power during the fabrication process is adjusted by choosing a distinct power value $P(d = 1.17\ \text{mm})$ for the first layer which is then reduced linearly to a power value of $P(d = 0.62\ \text{mm})$ for the last layer which is about 68 % of $P(d = 1.17\ \text{mm})$. This power correction was applied in order to fabricate the same scaffold structure as shown in Fig. 3, which is displayed in Fig. 5a. The power was adjusted from with $P(d = 1.17\ \text{mm}) = 2.50$–$P(d = 0.62\ \text{mm}) = 1.70$ mW.

Moreover, a large-scale scaffold was fabricated using the same approach. The result is displayed in Fig. 5b. The CAD model in Fig. 5d is designed to have a height of 4.7 mm and a diameter of 3.1 mm as well as cubic pores with a side length of 500 µm. As fabrication parameters, an objective with an NA of 0.45, a writing speed of 10 mm/s, hatch and slice distances of 10 µm, a spacer thickness of 5 mm, and laser powers $P(d = 5.17\ \text{mm})$–$P(d = 0.47\ \text{mm})$ between 5.5 and 3.5 mW were used. The total fabrication time was about 3.5 h.

Compensating the laser power, the scaffolds displayed in Fig. 5a, b show an excellent structural homogeneity along the z direction. The axial pore diameters are constant within each structure as are the overall lateral dimensions of the scaffolds.

The smaller scaffold shown in Fig. 5a was measured to have a height of ca. 520 µm and a width of ca. 480 µm. The axial pore diameter is around 75 µm and thus clearly smaller than the lateral pore diameter of ca. 95 µm. This is reasoned by the elongated voxel shape which leads to the axial resolution being lower than the lateral resolution.

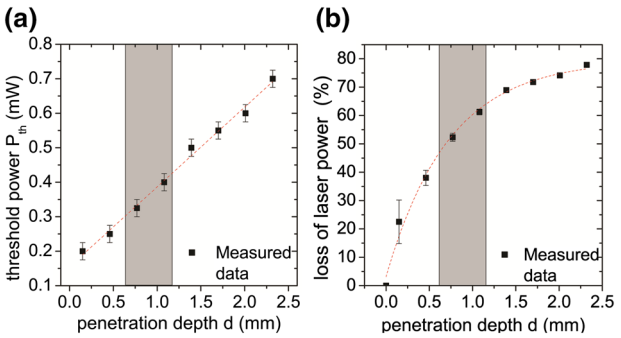

Fig. 4 **a** Threshold power P_{th} and **b** loss of laser power P_{loss} as a function of the penetration depth d for an objective with an NA of 0.60. The *gray shaded area* marks the process window for the scaffold production with a spacer thickness of 1 mm

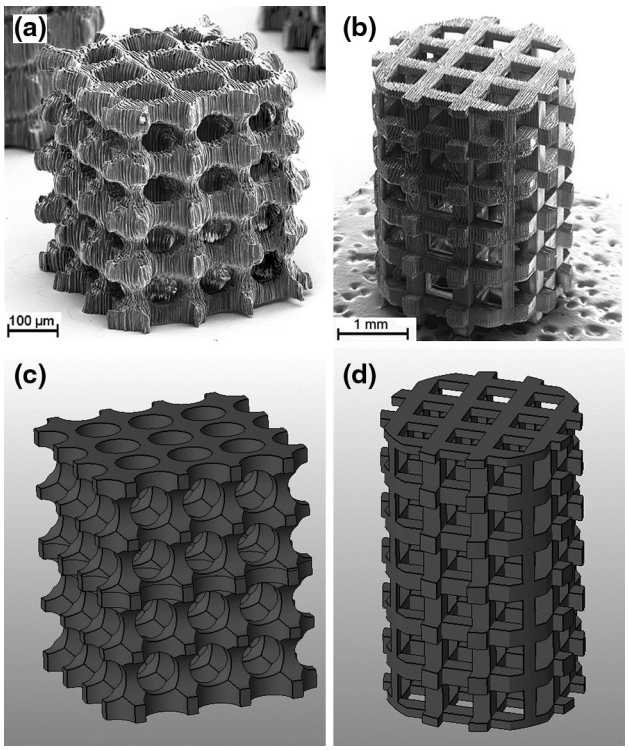

Fig. 5 **a**, **b** SEM images of scaffolds of different sizes, produced in OC-V (formulated with 2 wt% photoinitiator) using objectives with **a** an NA of 0.60, and **b** an NA of 0.45 and **c**, **d** corresponding CAD models

The large-scale scaffold of ca. 4.2 mm in height and ca. 2.9 mm in diameter is shown in Fig. 5b. The pore side length was measured to be around 480 µm in the lateral and 450 µm in the axial direction, thus showing the same anisotropy than observed with the smaller scaffold.

For both scaffolds the observed deviations of the overall dimensions compared to the CAD models are clearly lower than 10 %. This deviation is cause by distortion during the development process. Since an excellent structural homogeneity along the z direction is observed, the distortion must be uniformly along z.

5 Conclusion

In conclusion, high-quality millimeter-sized scaffold structures with interconnected pores were fabricated by 2PP using medium NA air objectives for biomedical applications. Compensation strategies to overcome the constraints of the point spread function spherical aberration were implemented into the process routine which take into account defocusing and blurring of the optical point spread function which are caused by refraction at the air/glass interface. Especially, blurring leading to reduction in the maximum peak power in dependency of the penetration depth was compensated in order to realize scaffolds with homogeneous geometrical and structural appearance along the z direction. The observed overall shrinkage which is below 10 % can be easily compensated by an adapted scaling of the CAD model before the fabrication.

Acknowledgments The authors gratefully acknowledge the Fraunhofer Gesellschaft für Angewandte Forschung e.V. (Challenge Program) and the German Science foundation (Grant: HO2475/3-1) for the financial support, and the excellent technical support of C. Cronauer and A. Martin (Fraunhofer ISC).

References

1. S. Kawata, H.-B. Sun, T. Tanaka, K. Takada, Nature **412**, 697 (2001)
2. R. Houbertz, Appl. Surf. Sci. **247**, 504 (2005)
3. M. Thiel, M.S. Rill, Freymann Gv, M. Wegener, Adv. Mater. **21**, 1 (2009)
4. R. Houbertz, H. Wolter, P. Dannberg, J. Serbin, S. Uhlig, Advanced packaging materials for optical applications: Bridging the gap between nm-size structures and large-area panel processing, In: *Proceedings of SPIE*, p. 612605, (2006)
5. B.H. Cumpston, S.P. Ananthavel, S. Barlow, D.L. Dyer, J.E. Ehrlich, L.L. Erskine, A.A. Heikal, S.M. Kuebler, I.-Y.S. Lee, D. McCord-Maughou, J. Qin, H. Rockel, M. Rumi, X.L. Wu, S.R. Marder, J.W. Perry, Nature **398**, 51 (1999)
6. A. Doraiswamy, T. Patz, R. Narayan, B. Chichkov, A. Ovsianikov, R. Houbertz, R. Modi, R. Auyeung, D.B. Chrisey, Biocompatibility of CAD/CAM ORMOCER polymer scaffold structures, In: *Materials Research Society Symposium — Proceedings*, vol. 845, p. 51–56 (2004)
7. R.J. Narayan, C. Jin, A. Doraiswamy, I.N. Mihailescu, M. Jelinek, A. Ovsianikov, B. Chichkov, D.B. Chrisey, Adv. Eng. Mater. **7**, 1083 (2005)
8. J. Li, B. Jia, M. Gu, Opt. Express **16**, 20073 (2008)
9. R. Houbertz, S. Steenhusen, T. Stichel, G. Sextl, in *Two-photon Polymerization of Inorganic–Organic Hybrid Polymers as Scalable Technology Using Ultra-short Laser Pulses*, ed. by Dr. F.J. Duarte. Coherence and Ultrashort Pulse Laser Emission (InTech 2010)
10. K. Obata, A. El-Tamer, L. Koch, U. Hinze, B.N. Chichkov, Light Sci. Appl. **2**, e116 (2013)
11. T. Bückmannn, N. Stenger, M. Kadic, J. Kaschke, A. Frölich, T. Kennerknecht, C. Eberl, M. Thiel, M. Wegener, Adv. Mater. **24**, 2710 (2012)
12. U. Streppel, P. Dannberg, C. Waechter, D. Michaelis, R. Kowarschik, A. Braeuer, Influence and utilization of UV-induced refractive index changes of photopolymers for the fabrication of 3D micro-optical elements, In: *Proceedings SPIE*, vol. 4991, p. 321 (2003)
13. K.H. Haas, H. Wolter, Solid State Mat.Sci. **4**, 571 (1999)
14. S. Schlie, A. Ngezahayo, A. Ovsianikov, T. Fabian, H.-A. Klob, H. Haferkamp, B.N. Chichkov, J. Biomater. Appl. **22**, 275 (2007)
15. G. Odian, Principles of Polymerization, 2nd ed. (Wiley, New York, 1981)
16. J. Serbin, A. Egbert, A. Ostendorf, B.N. Chichkov, R. Houbertz, G. Domann, J. Schulz, C. Cronauer, L. Fröhlich, M. Popall, Opt. Lett. **28**, 301 (2003)
17. M.J. Nasse, J.C. Woehl, J. Opt. Soc. Am. A: **27**, 295 (2010)